condensed matter

MDPI

Review

The Laser Powder Bed Fusion of $Nd_2Fe_{14}B$ Permanent Magnets: The State of the Art

Ivan Pelevin [1,*], Maria Lyange [1], Leonid Fedorenko [1], Stanislav Chernyshikhin [1] and Irina Tereshina [2]

[1] Additive Manufacturing Laboratory, National University of Science and Technology MISIS, 119991 Moscow, Russia; lyange.mv@misis.ru (M.L.); leonidjudo@gmail.com (L.F.); stanislav.chernyshikhin@skoltech.ru (S.C.)
[2] Faculty of Physics, Lomonosov Moscow State University, 119991 Moscow, Russia; irina_tereshina@mail.ru
* Correspondence: peleleq@gmail.com

Abstract: In recent years, significant effort was made to make the 3D printing of fully dense rare-earth permanent magnets a reality. Since suitable $Nd_2Fe_{14}B$-based initial powder material became available, additive manufacturing implementation spread widely, which led to many studies being focused on using this material in 3D printing. This study shows the principal possibilities of the synthesis of Nd-Fe-B magnets by means of the laser powder bed fusion technique; moreover, this study shows significant progress in increasing their magnetic properties. This progress was made possible by different approaches, such as 3D-printing process optimization, the addition of a second phase (a low-melting eutectic) into the initial powder, the tuning of the main phase's composition, and exploring different scanning strategies. However, the current level of material magnetic properties obtained via laser powder bed fusion is still far from that of magnets produced by using conventional powder metallurgy methods. The present review aims to capture the current state-of-the-art trials and highlight the main challenges.

Keywords: laser powder bed fusion; selective laser melting; hard magnetic materials; permanent magnets; rare-earth intermetallic; 3D printing; $Nd_2Fe_{14}B$; additive manufacturing

check for updates

Academic Editor: Annette Bussmann-Holder

Received: 30 January 2025
Revised: 4 April 2025
Accepted: 7 April 2025
Published: 24 April 2025

Citation: Pelevin, I.; Lyange, M.; Fedorenko, L.; Chernyshikhin, S.; Tereshina, I. The Laser Powder Bed Fusion of $Nd_2Fe_{14}B$ Permanent Magnets: The State of the Art. *Condens. Matter* **2025**, *10*, 22. https://doi.org/10.3390/condmat10020022

Copyright: © 2025 by the authors. Licensee MDPI, Basel, Switzerland. This article is an open access article distributed under the terms and conditions of the Creative Commons Attribution (CC BY) license (https://creativecommons.org/licenses/by/4.0/).

1. Introduction

The vigorous growth of modern technologies in aerospace, automotive, communication, military systems, and other novel applications [1,2] increased the demand for high-energy permanent magnets (PMs). Moreover, the requirements of the current market for the performance and shape variety of rare-earth PMs initiated the exploration of new production technologies. $Nd_2Fe_{14}B$-based PMs are vital to the various spheres of industry due to their record-high $(BH)_{max}$ of up to 474 kJ/m^3 [3], and the demand for rare-earth metals (REMs) in these industries is expected to continue to grow. Since the $Nd_2Fe_{14}B$ phase was discovered, the optimization of its synthesis and the production of items using this material have almost allowed the theoretically calculated limit of magnetic properties (93.4% of the theoretical value) to be reached in practice. Thus, modern scientific studies concerning this material are focused mostly on production cost reduction [4], increasing corrosion resistance [5], recycling [6,7], and theoretical investigations into new methods of treatment and additives using machine learning [8].

NdFeB permanent magnets are divided into sintered and bonded magnets. Sintered magnets are manufactured by using conventional powder metallurgical technology involving alloying, milling, pressing, and sintering. Most pressed and sintered magnets have basic geometries; hence, turning them into complex geometries is complicated and

expensive. Indeed, shaping magnets into complex, small, and precise parts is difficult when using conventional manufacturing processes because of their high brittleness. Thus, bonded magnets, composed of magnetic powder combined with a polymeric component, offer flexible formability and products with intermediate energy. Manufacturing-bonded magnets have greater flexibility than both classic techniques: sintered and hot deformation. Conventional technologies used for fabricating bonded magnets are powder injection molding (PIM), metal injection molding (MIM) [9], compression molding (CM) [10], casting, calendering, and extrusion processes (E&C) [11]. These methods allow for the manufacturing of complex and near-net-shape geometries but require special expensive equipment for each design. In this context, additive manufacturing (AM) and 3D printing emerge as innovative technologies for producing bonded magnets of customized shapes. AM offers several processing advantages: it allows the material to be used, hence reducing the amount of critical rare-earth magnet powders needed for printing, eliminating tooling needs, and reducing time costs [12]. Several studies have focused on technologies for recycling sintered magnets into bonded magnets [13,14].

The recent development of additive manufacturing techniques dealing with metallic powder as the initial material expanded the possibilities of designing and producing metal parts and opened up new scientific fields. Among a wide range of different AM techniques, one of the most common is laser powder bed fusion (LPBF), which represents the melting of the sample from powder layer by layer under laser irradiation according to a 3D computer-aided design (CAD) model [15]. The first LPBF process, selective laser sintering (SLS), was developed at University of Texas [16]. According to Ahmadi et al. [17], LPBF was first used in 1995 at the Fraunhofer Institute ILT in Aachen, Germany. Initially, the development of the LPBF technique took place mainly in the context of structural materials such as aluminum [15,18–20], titanium [21–26], nickel [27–31], cobalt [32,33], and copper-based [34,35] alloys. Steels are required for industrial needs [36,37]. Pure elements [38–44] are used for some specific applications, such as details for capacitors, space aircraft, and biomedicine. Along with the mechanical and special physical properties of 3D-printed samples coming into scientific focus, including the LPBF of rare-earth-based PMs, which combine the advantages of bonded and sintered magnets, was the ability to produce almost any shape and to achieve nearly full density without a non-magnetic binder material.

The LPBF method has a number of advantages and features for the production of metallic parts in general and for REM PMs in particular. It provides the highest accuracy among the AM methods for metallic materials and the possibility to obtain almost any shape and allows one to work with a wide range of materials [45]. In addition, LPBF is characterized by high cooling rates (10^4–10^6 K/s) and, consequently, rapid solidification due to the small size of the melt pool and the high temperature gradients during synthesis. In the case of Nd-Fe-B, it leads to a special microstructure of the material with ultra-fine grains, an order of magnitude smaller than that of sintered magnets and favorable for high coercivity. On the other hand, it produces residual stress, leading to shape distortion, cracking, and other defects. The presence of these defects strongly depends on the mechanical properties and microstructure features of the material used. So, as a rule, they are not detected in aluminum alloys with near-eutectic composition and high plasticity [46], whereas more brittle alloys often require more thorough optimization of the synthesis process because they are prone to cracking, distortion, and other defects [47].

The first successful 3D-printed $Nd_2Fe_{14}B$-based volumetric samples by means of LPBF was described by Jacimovic et al. in 2017 [46]. Since then, the development of the LPBF of $Nd_2Fe_{14}B$-based materials and their properties has come a long way; however, the achieved level of the properties is still far from that of magnets produced via conventional

technological procedures [48]. Various approaches have been proposed in order to improve the quality of the printed material and enhance its magnetic properties, including the double-exposure scanning strategy developed by the authors of [49], the addition of a second low-melting phase [50,51], alloy composition tuning [52], and others. The present review aims to summarize significant achievements in microstructural, magnetic, and mechanical properties in NdFeB manufacturing by LPBF, discuss possible paths for further improvements in LPBF-prepared materials based on $Nd_2Fe_{14}B$ rare-earth intermetallic phase, and emphasize the challenges of this method.

2. Initial Powder Materials

2.1. Powder Requirements

The active development of $Nd_2Fe_{14}B$ permanent magnet synthesis by means of AM techniques is impossible without an available and suitable raw material—initial powder—that meets specific requirements. In the case of LPBF, these requirements are known [15,53] and are detailed as follows.

The LPBF process imposes specific properties of powder particle size distribution (PSD), shape, density, flowability, and other powder morphology characteristics, which have considerable impact on the quality of the components. The powder parameters can be categorized as single-particle (shape, smoothness, PSD, impurities, composition, moisture, etc.) and bulk (apparent or bulk density, tap density, Hausner ratio, flowability, and physical properties) properties [48]. Thus, the availability of the proper initial powder material is one of the most important and main limiting factors of LPBF technology development.

Since the cycle of the scanning of each layer by laser irradiation includes the important step of powder layer formation, this powder should possess high flowability and tap density, which can be achieved with a narrow and specific particle size distribution (as a rule, 15–50 μm), and each particle should have a spherical shape. Particle sphericity is usually controlled by using scanning electron microscopy (SEM). SEM is also usually used for particle size distribution analysis with a laser particle analyzer. In addition to these requirements, the homogeneity of chemical and phase composition should be maintained for a smooth and continuous melting process. Deviation from this requirement both in distribution and/or in shape leads to a significant decrease in flowability and a low quality of powder layer formation. The result of using non-suitable powder for the LPBF procedure increases structural defects such as pores, voids, and lack-of-fusion regions. The quality of the initial material plays a major role in the printing procedure and properties of the final product. Shape, size, internal porosity, surface morphology, and composition are some of the relevant factors of the powder feedstock.

2.2. MQP-S Powder Grade

Jacimovic et al. [46] first used the LPBF technique for Nd-Fe-B material to print 3D structures in the year 2017. Cubic samples and ring-like samples with complex shapes and a relative density (RD) of 92% were synthesized. Microstructure investigations showed the presence of cracks, pores, and voids, resulting in relatively low RD. However, the fundamental possibility of applying LPBF to $Nd_2Fe_{14}B$-type materials was demonstrated and proved [54]. The magnetic properties of the samples demonstrated great prospects through this technique. The remanence B_r and $(BH)_{max}$ values at lower temperatures were slightly higher than the injection-molded references and substantially higher than the SPS-sintered magnets composed of the same powder. It should be noted that the technique was developed largely due to the creation of a suitable raw powder—MQP-S-11-9-20001 grade by Magnequench [55]—the only commercially available spherical magnetic powder. This

powder was first actively used for bonded magnet production, particularly by injection molding and extrusion; then, the scope of its application was expanded to LPBF.

Today, a significant part of studies in Nd-Fe-B additive manufacturing use Magnequench powder due to its availability and the possibility of reproducing results by using standardized raw material. According to the manufacturer, MQP-S powder is produced by gas atomization from the melt, which allows one to obtain an almost spherical shape for each particle [55]. The sifting procedure through a sieve system provides the desirable particle size distribution. An analysis of literature shows that there are no noticeable problems, defects, or deviations from the required characteristics of this material. However, it should be noted that the experimental studies performed by the authors demonstrated that a significant particle fraction has chippings [56]. The typical appearance of the powder is shown in Figure 1, where chipped particles are also seen. For the production of bonded magnets, other types of powder could be used, such as MQP-B-10118-70, MQP-B-20173-070, and XCN110A, with particles of spherical or flake form. Mapley et al. studied the influence of the particle form on the magnetic and mechanical properties [57]. The spherical morphology allows the maximum density to be reached and, consequently, mechanical properties with higher H_c and insignificantly lower B_r to be obtained. Thus, the spherical morphology is preferable, and the MQP-S powder fulfills this requirement.

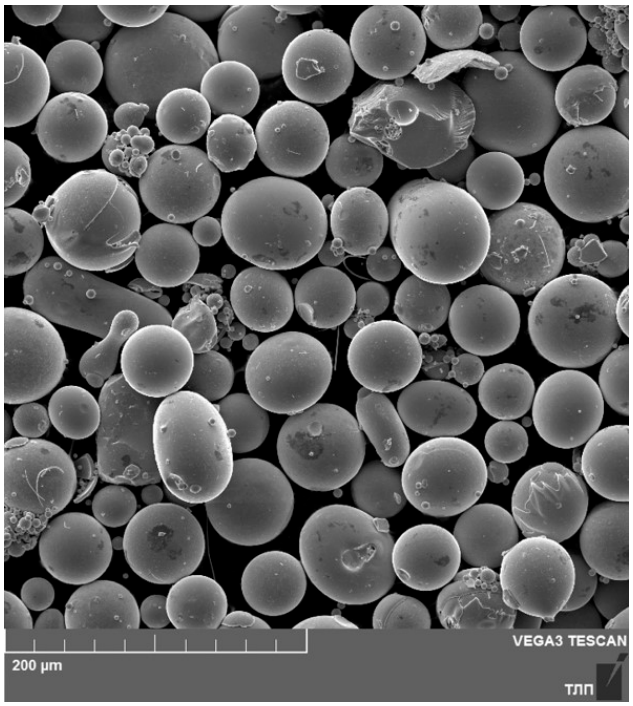


Figure 1. SEM image of MQP-S-11-9-20001 initial powder.

The chemical composition of the MQP-S powder does not match the $Nd_2Fe_{14}B$ stoichiometry and consists of Nd-Pr-Fe-Co-Ti-Zr-B elements. The compositions, both that given by the manufacturer and that measured by the authors, are given in Table 1. Some differences between passport and measured values could be because of errors that arose during EDX measurements, especially concerning lightweight elements like boron. The morphology is mainly spherical with a high proportion of small particles with size distributions of d50 = 38 µm and d90 = 65 µm and some agglomerates.

Table 1. Chemical composition of MQP-S (wt.%).

Element	Manufacturer's Data	Measured
Nd	17.2	17.0
Pr	1.9	1.9
Fe	69.8	66.8
Co	2.8	2.9
Ti	2.1	2.1
Zr	4.3	4.7
B	1.7	2.7
C	0.1	0
Cu	0.1	0

MQP-S has less RE element content than the stoichiometric 2-14-1 composition and far less than RE-rich alloys, which are usually used for conventional sintered magnets. An excess of RE leads to the formation of RE-rich phases along grain boundaries and positively influences the magnetic properties [58]. Thus, MQP-S material with low RE content seems not to be an optimal alloy to achieve a high-energy product of 3D-printed permanent magnets. This problem can be solved by adapting other alloys for the LPBF technique or optimizing the LPBF synthesis parameters; for instance, the enhancement in magnetic properties is possible [59,60]; However, we are still far from achieving this through conventional methods.

2.3. Alternatives to MQP-S Powder

A significant approach to achieving high magnetic properties is connected with another composition of the alloy compared with MQP-S material. Goll et al. [61] compared RE-lean, stoichiometric, and over-stoichiometric Nd-Pr-Zr-Ti-Co-Fe-B compositions and obtained high $(BH)_{max}$; However, the authors concluded that the optimization of the LPBF parameters was still needed to decrease porosity and fracture behavior and improve the microstructure.

A new method, called grain boundary diffusion (GBD) based on infiltration by RE-TM (transition metal) is emerging as an efficient technique to enhance H_c and, at the same time, keep the total RE content relatively low [62–67]. GBD is processed by infiltration powder with a low-melting paramagnetic alloy (i.e., NdCuCo and PrCuCo). The eutectic alloy performs two functions, namely, (i) densification and mechanical strength improvement and (ii) the increase in coercivity by the effective separation of the nanoscaled grains of the main hard magnetic phase that suppresses the exchange interaction between the grains. Recent progress of the GBD process was reviewed by F. Chen [68].

Huber et al. studied the influence of different low-melting eutectics by the additional grain boundary infiltration process after selective laser sintering [50]. Infiltration by Nd70Cu30, Nd80Cu20, and Nd60Al10Ni10Cu20 allowed the coercivity to be increased from 0.65 (522 kA/m) to 1.0 T (842 kA/m), whereas the use of Nd50Tb20Cu20 as the diffusion source resulted in a larger coercivity of 1.5 T (1215 kA/m) (see Table 2). According to [50] a Nd-rich phase formed at the grain boundaries of the Nd-Tb-Cu diffused sample, covering nanosized $Nd_2Fe_{14}B$ grains. A Tb-rich shell could be seen covering the surface of $Nd_2Fe_{14}B$ grains. No α-Fe was observed in the microstructure, which was thought to be due to the reaction of the Nd-Tb-Cu liquid phase with the Fe phase during the diffusion process. Unlike Nb, with Tb, the diffusion process occurs at temperatures of 850 °C, and with the Nd-Tb-Cu eutectic, it is carried out at temperatures of 650 °C.

Table 2. Summary data about infiltration by low-melting eutectic phases.

Infiltration	Powder	H_{cj}, kA/m	B_r, mT	Year	Ref.
	Powder MQP-S-11-9 (datasheet)	650–750	739–760		[55]
$(Pr_{0.5}Nd_{0.5})_3(Cu_{0.25}Co_{0.75})$	80% MQP-B (nano) with 20% Inf.	1280	N/A	2020	[51]
Initial sample	MQP-S-11-9	522.4	436	2019	[50]
$Nd_{50}Tb_{20}Cu_{30}$	MQP-S-11-9	1215.2	466		
$Nd_{60}Al_{10}Ni_{10}Cu_{20}$	MQP-S-11-9	862.4	390		
$Nd_{70}Cu_{30}$	MQP-S-11-9	842.4	464		
$Nd_{80}Cu_{20}$	MQP-S-11-9	778.4	475		

Volegov et al. [51] mixed MQP-B powder with (Pr0.5Nd0.5)3(Cu0.25Co0.75) eutectic powder (80:20 weight ratio) and studied the influence of grain size, namely, nanocrystalline (as delivered, grain size of 25 nm) and microcrystalline (after additional annealing at 1273 K, grain size of 450 nm). The nanocrystalline sample consisted of the initial $Nd_2Fe_{14}B$ magnetic phase, as well as several new phases, including α-Fe, (Nd, $Pr)_2O_3$, and (Nd, Pr)$(OH)_3$ phases. The highly coercive sample was nanocrystalline due to the irreversible rotation of the magnetization in the nanograins.

Zh. Toujun proposed the double-alloy method combining GBD in the production of sintered magnets. The core idea was adding Dy and Tb in different stages. First, a Dy-rich shell was formed (by adding TbH_3), and the coercivity improved; after that, the GBD of TbH_3 resulted in the creation of a secondary Tb-rich shell on the surface of the grains [69]. The enrichment of Tb in the GB phase reduced the corrosion rate and improved the chemistry stability of NdFeB magnets. Thus, the same method could be implemented in AT.

The latest study by Tosoni et al. [52] describes the development of Cu-rich Nd-Fe-B alloy and powder. The authors showed that even using a non-spherical initial powder of the developed alloy but with optimized composition allowed them to reach impressive results in coercivity enhancement, the highest so far. However, there was still insufficient remanence because of the lack of texture in the printed samples.

Based upon the provided results, grain boundary infiltration seems to be one of the most promising approaches to improving both the quality of the printed Nd-Fe-B-based materials (increase in density and reduction in defects) and coercivity through the magnetic isolation of grains, whereas the enhancement of remanence could be achieved by magnetic anisotropy formation. Perhaps, the combination of alloy composition tuning with the infiltration approach will give a synergistic effect and allow even higher coercivity to be obtained.

3. LPBF Process

3.1. LPBF Peculiarities

The combination of various AM methods potentially makes the procedure of PM production faster and cheaper and allows for the realization of complex shapes with minimum material losses, giving the possibility of creating localized material states or, specifically, the graded properties locally in the magnetic material. AM can realize the combination of special magnetic, thermal, electrical, and mechanical functionalities and enable workability at high temperatures. For example, Karl-Hartmut Müller proposed [48] the implementation of cooling channels inside a permanent magnet, which could allow the operational temperatures to be increased. The above option is not achievable when using conventional methods of powder metallurgy.

Among the AM techniques, LPBF is one of the most attractive for the production of fully dense metallic parts due to its high accuracy, the possibility of the fine-tuning of the process to adapt it to a wide range of materials, and the ability to synthesize items of almost any shape [15]. The LPBF process involves a series of steps, including powder layer deposition and laser scanning. It is conducted within an inert, controlled-atmosphere chamber to avoid oxidation during processing, i.e., melting and solidification, which is crucial when dealing with REM-containing materials. LPBF uses a high-energy laser beam to melt the metal powder completely along the laser path. By repeating this procedure and overlapping layer by layer, a three-dimensional component is formed. The layer-by-layer approach allows for complex structured and thin-walled components formation. Recycling the metallic powder increases the feedstock utilization rate and reduces the production cost. The laser interacts with the metallic powder to form a small molten pool on a scale of approximately 100 μm. The scheme diagram of the LPBF process is depicted in Figure 2. The cooling rates of the molten pool reach 10^4–10^6 K/s due to the high thermal gradients which occur during melting. Such rapid cooling rates inhibit grain growth and the segregation of the alloying elements. Together with the stirring action of Marangoni flow [19] in the molten pool, a fine microstructure that significantly influences the properties of the material is formed. The non-equilibrium solidification process increases the solid-solution limit of the alloy elements, and new metastable or even amorphous phases may occur. On the other hand, the large temperature gradients and complex heat transfer due to the cyclic processing of the laser beam usually result in the directional growth of grains, so the microstructure and properties of the alloy tend to be anisotropic. The high cooling rates lead to fine or even nanosized grain structure formation, which is favorable for high magnetic properties. The challenges of LPBF are structural defects such as porosity, cracks, shape distortions, and other defects which arise because of non-optimized process parameters, high residual stresses, and the high brittleness of the material.

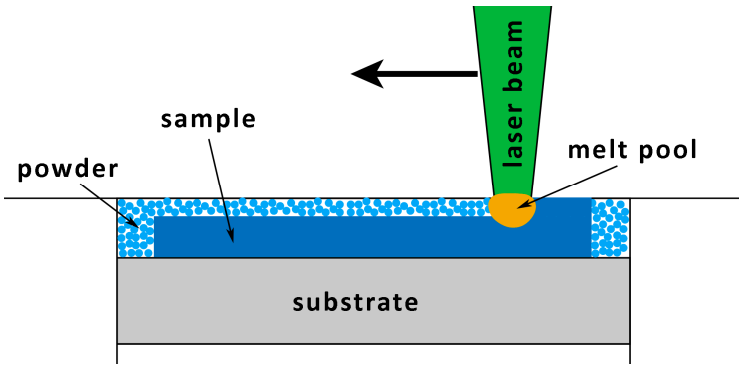


Figure 2. Scheme of LPBF process, where powder feed can be realized differently.

Numerous researchers have identified the influential process parameters for LPBF as laser input energy, powder material morphology, scanning speed, and others [70–72]. The melting process is influenced by the material characteristics, powder fluidity, particle size/shape/distribution, the type and spot size of the laser, etc. The use of improper process parameters may cause balling, pores, cracks, and low density. The features, peculiarities, challenges and perspectives of Nd-Fe-B-based 3D printing via the LPBF technique are described below.

3.2. LPBF Process Parameters

LPBF is a technology which allows for the fine-tuning of the melting process through the variation in its parameters. The process parameters can be divided into four categories: (1) laser-related parameters (laser power, spot size, wave-length, etc.); (2) scan-related

parameters (scanning speed, hatch spacing, and scan pattern (strategy)); (3) powder-related parameters (particle shape, particle size and distribution, powder bed density, layer thickness, material properties, etc.); (4) temperature-related parameters (powder bed temperature, powder feeder temperature, temperature uniformity, etc.) [47]. However, most of these parameters are interdependent, and the process of choosing parameters aims at finding a balance. For instance, the setting of the power of the laser is based mainly on the melting temperature of the alloy and absorption coefficient. The processing parameters can have a significant impact on the microstructure and consequently the mechanical and magnetic behavior of the alloys. Many reviews are devoted to the topic of processing and the influence of parameters in LPBF. For example, Sames et al. provided a processing map for the case of metal AM and discussed the challenges in magnetic material printing [72]; Aboulkhair et al. presented a detailed review of the AM methods and process parameters [15]; Chaudhary discussed the general principles of magnetic material printing [73] and more [54].

When heating and melting occur, the heat capacity and latent heat must be considered. These heat parameters are strongly dependent on the material and proportional to the mass to be melted. For instance, insufficient energy is usually a combination of low laser power, high scanning speed, and large layer thickness, which often results in lack-of-fusion defects and/or balling effect due to the lack of wetting and the remelting of the molten pool with the preceding solidified layer. However, high laser and low scanning speed may result in extensive material evaporation and the keyhole effect, leading to pore formation. The shape of the high-power laser beam, which might differ among lasers, defines the heat input distribution and melt-pool shape and dimensions. The typical reasons for crack formation during LPBF are very high thermal gradients (thermal stress cracking), the broadening of the solidification range during rapid solidification (solidification cracking or hot tearing), and the presence of rather brittle precipitates acting as stress concentrators (ductility dip cracking). Poor hatch spacing often results in regular porosity in the built parts, as adjacent melt lines do not fuse together completely. Vaporization within an LPBF machine may result in the condensation of volatilized materials on the laser lens, disrupting the delivery of laser power. Hence, a suitable combination of laser power, scanning speed, hatch spacing, and layer thickness is essential for LPBF processing to successfully build near-full-density parts.

One of the quantitative parameters which is commonly used for characterizing the energy input during the process is energy density (ED). It can be calculated based on a linear, areal, or volumetric approach, where the latter is the most used in the literature. The linear energy density (ED_l, J/mm) is calculated by using the formula

$$ED_l = \frac{P}{V}, \tag{1}$$

where P is the laser power (W) and V is the scanning speed (mm/s). The areal energy density (ED_a, J/mm^2) further considers the hatch spacing (h, mm) as follows:

$$ED_a = \frac{P}{V \cdot h}. \tag{2}$$

Areal energies below 0.6–0.8 J/mm^2 (in the case of Nd-Fe-B AM) allow for the sintering of powder particles, which results in slightly consolidated, highly porous samples [59]. Increasing the areal energy from 0.8 to 2.3 J/mm^2 allows for a uniform LPBF process and results in outwardly intact bulk samples. Increasing the areal energy results in delamination within the sample. Furthermore, it was found that a laser power of 200 W or more is, in

general, unsuitable for the LPBF of Nd–Fe–B [74], but this result cannot be generalized to other LPBF machines [49].

The most used form of energy density in the literature is the volumetric energy density (ED_v, J/mm^3), which is calculated as follows:

$$ED_V = \frac{P}{V \cdot h \cdot t} \quad (3)$$

where t is the layer thickness (mm).

3.3. Density and Scanning Strategies

In the literature, it is customary to operate with the concept of relative density (RD), which is calculated as the ratio of the actual density to the theoretical density of the material and is expressed as a percentage. In the case of structural materials, a satisfactory ED is usually considered to be at least 99.5%, but in the case of Nd-Fe-B intermetallic compounds, such density level is extremely difficult to achieve due to their brittleness and low processability. The best values of RD achieved lie in the 90–95% range in most studies. Skalon et al. achieved a relative density of 90.87% [75] by treating a layer of powder of constant depth. The maximum relative density was obtained with the following parameter settings: a power of 60 W, a laser speed of 160 mm/s, and a hatch spacing of 500 µm. Similar results were obtained by Kim et al. [76]—the highest RD was 90.2%. Urban et al. investigated the influence of process parameters on relative density and polarization [60] (for the experiments, layer thickness and hatch distance were fixed to 20 µm). As polarization depends on the amount of active material in the volume, there is a clear correlation between density and polarization. A small region of high RD (up to 94%) and polarization with parameter settings from 40 to 55 W and from 1200 to 2000 mm/s can be identified.

Separate important factors can be identified with a laser scanning strategy. It is known that the scanning strategy influences microstructure features, texture, grain structure, and anisotropy and thus the properties of printed materials [49,61,77,78]. The most common scanning strategy is performing a 67° rotation between adjacent layers (see Figure 3a) and dividing the scanning area into chess squares (islands). There are some more common scanning strategies, like 90° rotation (Figure 3b), scanning only in one direction (no power during returning) and in both directions (straight and opposite), special scanning techniques for edges, etc. In most studies concerning Nd-Fe-B 3D printing, the scanning strategy is not discussed, which means that one of the default strategies offered in the equipment software application is used. However, some interesting results concerning this point should be noted. The specific scanning strategy approach was applied by Goll et al. [61] to obtain textured FePrCuB samples. The strategy represented linear parallel trajectories of the laser spot with opposing directions for neighboring tracks (forward–backward). In that study, a strong influence on the microstructure and shape of the grains was shown, especially after subsequent heat treatment (one more possible way to improve printed material properties), by thorough optical and electron backscatter diffraction. The resultant textured microstructure with elongated grains, expectedly caused magnetic anisotropic properties: the significant difference in remanence measured along the different axes was shown. Tosoni et al. [52] described the strategy using a 90° rotation and scanning only in one direction. Moreover, it is noted that some samples were printed without rotation; however, there was neither a comparison nor any discussion about the influence of the strategy on the microstructure and properties.

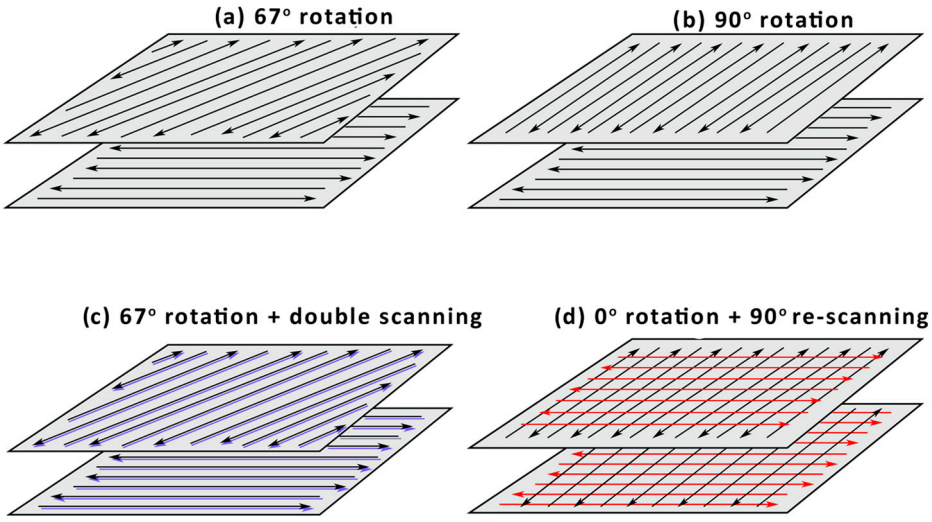


Figure 3. Schemes of various scanning strategies, where the arrows indicate the scanning paths of the laser beam.

In the previous study conducted by the authors, a new scanning strategy was proposed [49], the double-scanning strategy, i.e., every powder layer was scanned twice (see Figure 3c). Two variations of the strategy were performed: (1) full-power laser exposure with subsequent half-power laser exposure and (2) half-power preliminary exposure with subsequent full-power scanning. The proposed scanning strategy allowed for a better melting process, leading to better quality of the printed samples, i.e., higher relative density (RD) of the synthesized material, compared with the basic single-exposure strategy (using the same LPBF parameters). High-density samples with RD values of up to 96% were obtained due to the internal stresses being decreased, thus reducing the volume of voids and cracks. The appearance of the samples obtained with the double-scanning strategy are shown in Figure 4. Thus, the possibility of a significant improvement in 3D-printing quality, as well as the influence on microstructure and magnetic properties, when using a specific scanning strategy was shown.

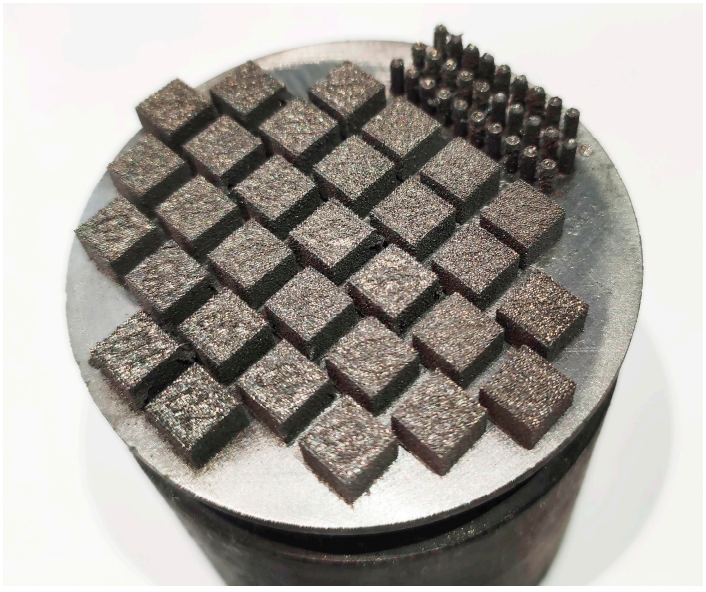


Figure 4. Cubic (5 × 5 × 5 mm) and cylindrical (1.5 × 5 mm) samples obtained with LPBF by the authors with the double-scanning strategy.

In [79], four scanning strategies were compared: 0°, 67°, and 90° rotation between adjacent layers and the double-scanning strategy (0° between adjacent layers and 90° between the first scan and the re-scan; see Figure 3d). The latter allowed for a significant improvement in the RD of 5–12%, allowing it to reach a level of ~95%; however, this did not result in an increase in residual magnetization and coercivity. It is worth noting that all printing processes were carried out at an increased substrate temperature of 80 °C, so a direct comparison between the results with other studies without substrate preheating is not possible. Thus, despite the described achievements, the topic of the laser scanning strategy's effect on Nd-Fe-B-based materials' structure and properties is still not fully understood.

The topic of the LPBF process with substrate preheating is also not fully studied. Finding the optimal balance between rapid solidification, which results in nanosized grains and thermal gradient, and cracking decreasing seems to be a promising way to improve the quality of printed Nd-Fe-B magnets. Except for the mentioned study [79], there is only one more study which is focused on this topic [80]. The substrate temperature dependence of RD was examined within the 300–550 °C range, and improvements in the density and remanence of the samples produced with preheating—approx.. from 90 to 94% and from 0.61 to 0.76 T, respectively—were observed.

Another not-well-studied topic is the heat treatment after 3D printing. Tosoni et al. [52,81] applied a heat treatment similar to convenient powder metallurgic processing, and the process was described; but there is a lack of discussion, and no dependency of the properties on the treatment process nor their trends were given. Bittner et al. [59] declared that the obtained high-coercivity state was achieved without any post-treatment, whereas Goll et al. [61,82] found an optimized two-step heat treatment which allowed high coercivity and remanence to be obtained. Despite the described results, there is no comprehensive investigation of a heat treatment application in LPBFed $Nd_2Fe_{14}B$-based materials; however, the implementation of such investigation is difficult because of the variation in material composition, i.e., a specific study is needed for each composition.

4. Microstructure and Defects

4.1. REM-Lean MQP-S Material

The magnetic properties of any permanent magnet material depend on its microstructure. As it was mentioned above, the LPBF method has its own characteristics, which affect microstructure formation: a short life-time of the molten state, high cooling and crystallization rates, etc. These peculiarities often lead to the formation of defects such as pores and cracks even in materials with high processability [83], and for REM-based intermetallic compounds, it is much more significant. In the case of structural material synthesis, the effect of defects on mechanical properties is usually investigated [84], whereas for NdFeB printing, the main problem of obtaining a fully dense material still remains, since it tends to crack and form pores and voids. The typical state of as-built samples synthesized by the authors from MQP-S alloy is shown in Figure 5. Lots of cracks and voids are seen, the formation of which is explained by the low processability of the material for LPBF (low mechanical properties, crystallization and phase composition peculiarities, etc.). Moreover, the microstructural analysis of $Nd_2Fe_{14}B$-based materials needs large volumes of experimental work along with high-precision equipment, so it is not surprising that some studies contain descriptions of only synthesis procedures and magnetic properties without microstructural analyses [60,74]

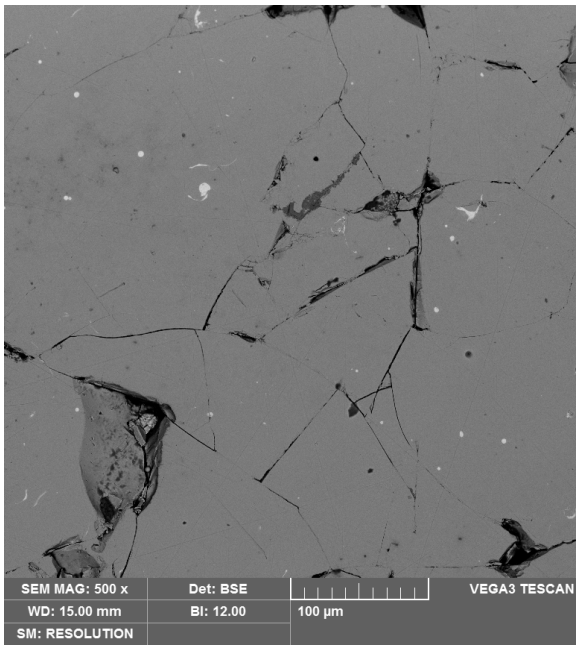


Figure 5. The SEM image of the polished surface of an MQP-S sample synthesized by the authors via LPBF.

Considering the MQP-S alloy, an REM-lean alloy composition microstructure with a $Nd_2FE_{14}B$-type phase along with Fe is expected. The presence of iron in most cases reduces remanence and coercivity due to its soft magnetic properties. However, the size of Fe inclusions and their fraction play a significant role in the final properties. In the first study performed by Jacimovic et al. [85], the analysis of the process parameters' effect on the microstructure of MQP-S materials was conducted. Special sensitivity of the structure and magnetic properties to the scanning speed was found. According to the study, the low speeds led to the formation of Fe and $Nd_2Fe_{14}B$ phases, along with Nd oxides. The iron had dendritic structure with a size of up to 30 µm, whereas the RE phase had an irregular shape of about a micrometer in size. The scanning speed increase resulted in a twofold reduction in the size of the Fe segregations, which had a very positive effect on the properties. It is worth noting that the study utilized equipment with a laser of low power of up to 120 W, which is lower than that used in most modern LPBF equipment.

Equipment with laser of even lower power (40–60 W) was used by Skalon et al. [75] to obtain volumetric samples from MQP-S powder. The layer thickness effect on the microstructure and properties was investigated at a laser power and scanning speed of 60 W and 160 mm/s, respectively. The grain size varied from 0.5 to 3 µm, depending on the layer thickness (the smaller the layer, the smaller the grain), which is less than the typical grain size after sintering and slightly higher than that in hot-pressed and hot-deformed materials. No dependance of chemical and phase composition of the samples on layer thickness was found; thus, it was concluded that the main factor influencing the magnetic properties is the grain size. A more recent study [76] used MQP-S material, and a $Nd_2Fe_{14}B/\alpha$-Fe nanocomposite structure was found. Sufficiently fast cooling rates and low ED values resulted in the crystallization of the nanosized 2:14:1 grains separated by an iron-rich soft magnetic amorphous grain boundary phase, which restricted coercivity. The logical conclusion made was that in order to enhance the coercivity, adjusting the powder composition was needed to obtain a non-magnetic grain boundary phase, which would isolate hard magnetic 2:14:1 grains, hindering remagnetization.

4.2. Other Materials

The formation of soft magnetic iron as a second phase in the structure utilizing REM-lean MQP-S alloy prompted the development of alternative materials for LPBF synthesis. Goll et al. [61] prepared an Fe73.8-Pr20.5-Cu2.0-B3.7 (at%) alloy. In the as-built state after LPBF, the samples consisted of fine crystals of Pr2Fe14B phase (matrix), as well as Pr-rich and PrCu-rich ones. The subsequent heat treatment (homogenization at 1000 °C for 5 h with slow cooling and aging at 500 °C for 3 h with slow cooling) led to the growth of Pr2Fe14B and Fe17Pr2 grains and their transformation into a polygonal form (the average grain size was 12 μm). The grain boundaries were filled with Fe13Pr6Cu1 and Pr-rich and Pr/PrCu phases. Additionally, the LPBF process and the applied heat treatment allowed the authors to obtain the partial texture of the material, which is crucial to remanence (more details about magnetic properties are in the next section).

The study of Nd-Pr-Dy-Fe-B-Co-Al-Cu-Ga alloys with excessive REM content was performed by Caniou et al. [81]. A few alloys with variable composition were prepared, cylindrical samples were synthesized via LPBF and annealed at temperatures between 400 °C and 700 °C with a cooling rate of 30 °C/min, and their structure and properties were analyzed. It was discovered that in the as-built state, the material consisted of both dendritic (closer to melt-pool boundaries) and equiaxed (in the centers of the melt pools) structures. The ratio of the structures depended on the alloy composition and LPBF energy density. The addition of Cu improved the wettability of the hard magnetic phase, forming a low-melting eutectic and decreasing the grain size. The Cu addition of 0.8 wt.% led to fine grain size (<10 μm) formation, which, along with the magnetic separation of $(Nd,Dy)_2Fe_{14}B$ grains by the RE-rich phase, provided high coercivity. The effect of ED_V on the microstructure was also investigated. At relatively low ED_V values, almost no iron dendrites were found, whereas higher energy gave enough time for Fe dendrites to induce a decrease in coercivity. A two-step 600 °C + 470 °C thermal annealing was found as optimal in order to enhance the magnetic properties due to the removed iron dendrites, along with the absence of grain growth.

An alternative approach to improving the quality and properties of Nd-Fe-B-based materials synthesized by LPBF is the addition of a second low-melting eutectic phase to the initial powder. Nd70Cu30, Nd80Cu20, Nd60Al10Ni10Cu20, and Nd50Tb20Cu20 eutectic phases were prepared by Huber et al. [50] and used for a grain boundary infiltration process at 650 °C for 3 h under vacuum. This produced fully dense samples and enhanced coercivity greatly by the magnetic isolation of the main phase's grains by the eutectic phases, especially in the case of the Nd-Tb-Cu eutectic. No Fe phase was observed in the microstructure after infiltration; the authors attributed this to its reaction with RE-rich liquid during the diffusion process. A similar approach was shown by Volegov et al. [51]. Non-spherical MQP-B powder under two conditions (nanocrystalline and microcrystalline) was taken, and a 20 wt.% (Pr0.5Nd0.5)3(Cu0.25Co0.75) eutectic alloy was added; the obtained mixture was used as a raw powder for LPBF. The presence of the following phases was found: $Nd_2Fe_{14}B$, α-Fe, (Nd, Pr)O3, (Nd, Pr)(OH)3, and (Nd,Pr)Fe4B4. Fe-rich crystals were located mostly in the upper layers of the microcrystalline sample, whereas the middle and bottom layers were almost Fe-free. The main phase's grain size was 1–3 μm for the microcrystalline sample and 100–200 nm for the nanocrystalline one.

4.3. Latest Achievements

More recent studies largely confirmed the described data and revealed new information. Genç et al. [80] provided comprehensive results of influence of the LPBF process parameters on the microstructure and magnetic properties of the MQP-S material. Additionally, powder bed heating was applied to improve the quality of the synthesized material

and its magnetic properties. The heating process increased the relative density from 90 to 96%. Remanence also tended to increase with the heating; coercivity, on the contrary, decreased. The correlation between density and magnetism was unidirectional: high magnetism implied high density, but high density did not necessarily mean high magnetism. This study confirmed again that the magnetic properties depend on the volume of the magnetically soft α-Fe phase. Another research study performed by Wu et al. [86] also describes the LPBF of MQP-S powder and the obtained microstructure and properties. In-depth grain structure analysis was conducted and correlated to permanent magnetic performance. It was shown that nanostructured $Nd_2Fe_{14}B$ grains and amorphous Ti-rich iron-based grain boundary phases primarily determine magnetic performance, while precipitates can potentially weaken magnetism. Remelting during processing helped to transform coarse grains into finer structures, improving the magnetic characteristics.

A comparative study of LPBF and laser-directed energy deposition (LDED) using MQP-S powder was conducted by Yao et al. [87]. The formation of a nanocrystalline microstructure after LPBF due to high cooling rates, which was beneficial for the magnetic properties, was shown in contrast to LDED and cast samples. $Nd_2Fe_{14}B$ grains varied in size from 50 nm to 2 μm depending on the location within the melt pool. A higher volume fraction of the $Nd_2Fe_{14}B$ phase and a lower content of α-Fe were found in the LPBF-produced material than in the LDED-produced one. Similar results to those previously described were obtained by Ming et al. [81]. A set of samples was synthesized by using various scanning strategies. Nd2Fe17Br phase and soft magnetic α-Fe phase were detected in the as-built sample. Significant inhibition of α-Fe formation was achieved by applying unidirectional, bidirectional, and contour scanning strategies. Moreover, the bidirectional strategy led to a high relative density of 97.1% and the highest magnetic properties among the obtained samples, which were attributed to higher cooling rates during solidification and the formation of a finer grain structure.

Nd-Pr-Ce-La-Fe-Zr-B powder was used by Dong et al. [79]. Despite the irregularly shaped particles of the powder, an RD of up to 95% was achieved. The formation of ~13–19 wt.% α-Fe along with 2-14-1 phases was also observed, where the content depended on the synthesis process. Cracks, pores, and voids were present in the obtained samples regardless of the process; however, applying the scanning strategy with low energy density remelting resulted in an increase in RD of 5–12%. Thorough grain orientation analysis using electron backscatter diffraction (EBSD) was carried out, and the mechanical properties of the LPBF-produced samples were estimated.

The present review of the studies focused on the microstructure features of Nd-Fe-B-based materials synthesized by the LPBF method shows information fragmentation despite several attempts to conduct comprehensive research. This could be explained by the variation in raw material composition and the high sensitivity of microstructures (and properties) to the composition, synthesis process, and subsequent treatment. Thus, comprehensive investigations on the topic are still needed in order to determine the dependency of the microstructure and properties on LPBF parameters. This seems one of the most important and promising directions for further studies in the field.

5. Magnetic Properties

5.1. LPBF vs. Conventional Methods

When investigating magnetic properties, we operate with characteristic properties of the hysteresis loop, such as maximum energy product $(BH)_{max}$ (kJ/m^3), remanence B_r (T), and coercive field H_{cj} (A/m). Two coercivity parameters are used to grade magnetic hardness: one is intrinsic coercivity, defined by the polarization curve $J = f(H)$, H_{ci} (or H_{cj}), and the other is normal (or technical) coercivity, H_c. Permanent magnets suitable for motor

applications must have high coercivity, and ideally H_{ci} is much higher than H_c, which allows the magnets to have a linear demagnetization induction (B) curve in the second quadrant [88]. The linear B curve is a very important characteristic that enables the magnets to be stable during operation.

NdFeB permanent magnets show outstanding performance, superior to previously discovered hard magnetics like Alnico and hard ferrites (B_r higher than 1T, H_c > 1000 kA/m, and energy product $(BH)_{max}$ > 200 kJ/m^3). NdFeB permanent magnets exploit this potential and cannot be further improved much. Today, in view of the expected increasing demand in strong sintered Nd-Fe-B magnets, there are two important goals, where the first is producing complex, net-shape PMs and the second is reaching performance stability at elevated temperatures up to 200 °C [89] and high coercivity for motor applications.

Conventionally, magnet production is realized by the powder metallurgical route, consisting of powder fabrication, pressing and magnetic field alignment, sintering, and post-sintering heat treatment [90]. A comparison of the extrinsic properties of magnets obtained by different methods is illustrated in Table 3. The maximum energy product is achieved by the conventional method of sintering. Hot-pressed magnetoplasts obtain a lower energy product but are easily treated and cheaper then sintered magnets. Hot-pressed magnetoplasts can replace sintered magnets in spheres, where high coercive force and energy product are not obligatory, magnetic separators, generators, sensors, etc. Bonded magnetoplasts, a kind of new-generation composite material made from permanent magnetic powder and plastic, have outstanding magnetic properties and plastic properties and feature high precision and exceptional shock resistance. Unlike NdFeB bonded compressed magnets, bonded magnetoplast NdFeB magnets can be processed into various components with complicated shapes, allowing the magnets to be used within more complicated applications. The additive manufacturing of NdFeB offers an opportunity to produce components of complex geometry, efficiently use material, and specifically tailor properties. As is seen from Table 3 and the diagram in Figure 6, AM magnets obtain lower energy product and residual induction and are still being investigated in laboratories.

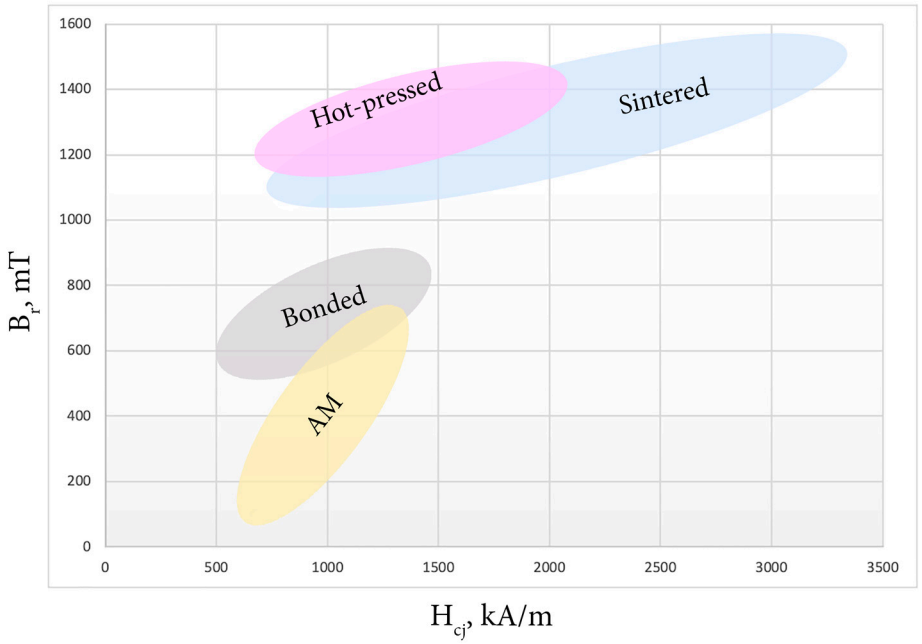


Figure 6. Coercivity/residual induction diagram for Nd-Fe-B materials obtained via different methods.

Table 3. Characteristic of permanent magnets, produced by different methods.

Production Method	$(BH)_{max}$ (kJ/m^3)	H_{cj} (kA/m)	B_r (mT)	Advantages	Disadvantages
Sintered	205–434	874–3180	1100–1500	• High magnetic properties	• High cost • High losses during production • Brittleness
Hot-pressed magnetoplasts	118–331	795–1987	1200–1400	• Corrosion resistance	• Only circle form • High technological barrier
Bonded magnetoplasts	47–94	556–1431	600–800	• Ability to prepare complex forms • Corrosion resistance	• Low magnetic properties • Low working temperatures
Additive manufacturing	42–64	675–1280	100–700	• Ability to prepare complex forms	• Method is being adapted

An innovative method of energy product enhancement is GBD [50,90–92], which has already been mentioned and discussed in previous sections. The process was proposed in 2005 and was proven to offer a high level of H_{cj} [90,91], later realized in industry. This process is studied in detail in previous reviews [62,86,87]. Now, most commercial Nd-Fe-B magnets with H_{cj} > 1600 kA/m are fabricated by GBD. The grain boundary diffusion process using low-melting-point eutectic alloys (i.e., Nd-Cu, Pr-Cu, Pr-Cu-Co, etc.) has been widely utilized to enhance intrinsic coercivity in melt–spun nanocrystalline ribbons [93], sintered magnets [3], hydrogenation–disproportionation–desorption–recombination (HDDR) powders [89,94,95], and thin films [96]. The main idea is that a thick rare-earth-rich and iron-deficient phase is essential to weakening the exchange coupling between $Nd_2Fe_{14}B$ grains, resulting in enhanced coercivity. The maximum working temperatures can be greater than 150 °C. The GBD process is used narrowly for the production of magnets with requirements of high magnetic properties and enhanced mechanical stability; otherwise, conventional methods are used [81].

Despite the lower level of magnetic properties of LPBF magnets compared with the ones obtained via conventional methods, the development of a fully dense 3D-printed magnet is ongoing with significant achievements. Huber et al. showed that the low coercivity of the sintered samples (without infiltration) is a result of the absence of the Nd-rich grain boundary phase which separates nanosized $Nd_2Fe_{14}B$ grains, as well as the existence of soft α-Fe phase in the microstructure. Infiltration leads to coercivity increase due to the formation of REM-rich phase [50]. The enrichment of Tb at the interface of the 2:14:1 grains increases the magnetocrystalline anisotropy field, hindering the nucleation of reversed domains at the interfaces and resulting in an increase in coercivity.

Volegov et al. [51] noted that introducing paramagnetic infiltration leads to higher coercivity values but also results in lower magnetization. Since the infiltration influence on magnetization depends on the area of the boundaries, the grain boundaries' volume that appears during infiltration can be reduced by a coarse grain size. Thus, nano- and microcrystalline magnets were synthesized and studied to investigate the influence of the microstructure on the magnetic properties of 3D-printed materials. It was found that microcrystalline magnets demonstrate lower coercivity (1.7 times less) in comparison with the nanocrystalline ones. This was due to the existence of large areas of magnetically coupled grains with shared boundaries in the 3D-printed microcrystalline magnets. Due to the coupled grains, the domain wall can easily move through the shared boundaries, leading to a reduction in coercivity.

5.2. Dependance of Magnetic Properties on Process Parameters

The magnetic parameters strongly depend on the melt-pool behavior in the range of parameters, which plays a great role in the density of the product, defects (pore and cracks), and smooth-surface formation. A nanocrystalline material with good magnetic properties could be produced with a shallow melt-pool depth of 20 to 40 µm. Skalon et al. [75] achieved one of the highest remanence values of 600 mT (Table 4) by using this parameter. However, it is worth mentioning that the energy input of the next layer affects grain growth in this heat-affected zone. It is in accordance with B. Chang [97], who studied the influence of laser spot welding on the microstructure of sintered NdFeB. Welding leads to the deterioration of magnetic properties in the nugget and the heat-affected zone. Thus, it is important to find the proper process parameters for the local powder to fully melt. Coercivity depends on the grain size. Like nanocrystalline magnets, a smaller grain size is beneficial for higher H_{cj} [75].

Table 4. Summarized parameters and magnetic properties of AM samples.

Machine	Process Parameters					Material	Magnetic Properties			Ref.
	P, W	Scan Velocity mm/s	Spot Size, µm	Layer Thickness, µm	Hatch Spacing, µm		$(BH)_{max}$, kJ/m^3	H_{cj}, kA/m	B_r, mT	
						Powder	72.6	706	710	
M2 LPBF machine	50–150	1000–2500	110	30	35–75	MQP-S	63	921	630	[59]
TruFiber 1000	200	2000	46	50	30	Nd-Pr-Zr-Ti-Co-Fe-B	64	384	690	[61]
AddSol D50	50, 100	1400	80	30	100	MQP-S	19	405	416	[49]
Farsoon FS121M	60	160	80	20	500	Nd-Pr-Fe-Co-B-Zr-Ti	55	550	600	[75]
SLM125	150	750	70	50	70	Nd-Pr-Dy-Fe-(CoCuAlGa)-B	38	551	550	[52]
AM125	-	-	40	30	100	MQP-S	63	921	630	[86]
Farsoon S121M	20–100	50–2000	100	20	-	MQP-S	-	1210	430	[50]
Aconity3D	-	-	100	-	-	MQP-B+Inf	-	1280	-	[51]
Mlab Cusing R Gen.1	55	1800	-	-	-	MQP-S	-	-	564	[60]
Model Realizer SLM 50	120	270	15–30	20	100	MQP-S	45	-	700	[85]
E-Plus-3D M100T LPBF system	160	1200	82	-	80	LW-N-400	13.8	205.8	139	[79]
Aconity Mini	130	3500	-	20	20	MQP-S	-	700		[80]
Commercial LPBF machine Guangzhou Xinyuan Metal S & T Co	100	1200	-	30	100	MQP-S	62	853	700	[20]
BLT-S210 system	120	1400	-	30	100	MQP-S		656	790	[87]

Goll et al. studied the effect of heat treatment on hard magnetic properties [61], without the need for subsequent powder metallurgical processing or rapid quenching. After traditional two-step annealing (step 1: homogenization at T = 1000 °C for 5 h followed by slow cooling to RT; step 2: annealing at 500 °C for 3 h followed by slow cooling to RT) known from as-cast magnets, the printed parts showed good magnetic properties, as seen in Table 4. The formerly present α-Fe is dissolved during heat treatment and is therefore not detected in the annealed state. Printed sample L-PBF-a contains additional RE oxides that are locally observed. Similar oriented grains reaching the texture grade of $J_r/J_s \approx 0.67$

increase remanence. Laser parameters leading to extremely rapid solidification during PBF-LB, combined with post-process annealing, were found to be important in obtaining a high-coercivity microstructure (the formation and wetting of the RE-rich grain boundary phase). Earlier, L. Schafer obtained the same result concerning annealing and enhancing magnetic properties [98].

Volegov et al. showed [51] that the ratio of coercivity values of the nanocrystalline magnet and the initial MQP-B powder $H_c{}^B/H_c{}^{\text{MQP-B}}$ is about 1.7, which is higher than that in the work by Huber [50] (1.15). This means that the 3D-printed permanent magnets produced by the proposed process can withstand a higher magnetic field compared with the original material without magnetization reversal.

The selection of scanning strategies is a crucial factor in manufacturing $Nd_2Fe_{14}B$, as they not only determine the spatial distribution of energy within the material but also regulate factors such as temperature gradient dynamics, thermal stress accumulation, and microstructural evolution. Consequently, the magnetic properties could be controlled by the scanning strategy. Pelevin et al. studied the effect of double exposure on the density and magnetic properties of $Nd_2Fe_{14}B$ with Nd70Cu30 addition material. The technique allowed a high-density, textured material (98.8%) to be obtained; however, it only led to the preservation of the magnetic properties, not to their significant improvement. Dong et al. found that the scanning strategy of $Nd_2Fe_{14}B$ grains with an interlayer transition angle of 67° performed the best for magnetic orientation [79]. The scanning strategy with an interlayer transition angle of 90° led to the best C-axis orientation and the smallest average grain size and therefore to the best magnetic properties, with an energy product of 13.8 kJ/m^3. Wu et al. achieved $(BH)_{max}$ = 62 kJ/m^3 by using a bidirectional scan strategy with a rotation of 67° between layers [86]. Thus, the scanning strategy is also a governing factor for enhancing magnetic properties.

Ming et al. [20] explored the influence of bidirectional, unidirectional, contour, and island strategies of scanning on density and magnetic properties. The unidirectional and bidirectional scanning strategies resulted in the highest magnetic parameters (see Table 4), simultaneously saving stable density parameters equal to 96.4% and 97.1%, respectively. Also, Ming et al. noted that numerical results showed that the cooling rate of the bidirectional strategy is relatively high during the LPBF process, which promoted grain refinement and explains the high values of the magnetic properties.

Yao et al. [87], in 2024, tried to enhance the magnetic properties by using preheating and a special scanning strategy with a reciprocating pattern between hatches and a rotation angle of 90° for the adjacent layers. Relatively high coercivity and remanence were linked with the presence of a considerable volume fraction of the $Nd_2Fe_{14}B$ hard magnetic phase, with columnar grains with a length of approximately 2 μm on the boundaries, along with globular $Nd_2Fe_{14}B$ grains ranging in size from 50 nm to 1 μm located inside the melt pools.

The summary diagram of the achieved main magnetic properties is presented in Figure 7, which shows the primary results.

In conclusion, the authors have shown the possibility to produce magnets with LPBF with high coercivity compared with sintered magnets. Both a technological and a fundamental understanding of the parameter influence and magnetization reversal processes of 3D-printed magnets open up the way for the additive manufacturing of high-coercivity and low-weight magnetic systems compared with sintered magnets.

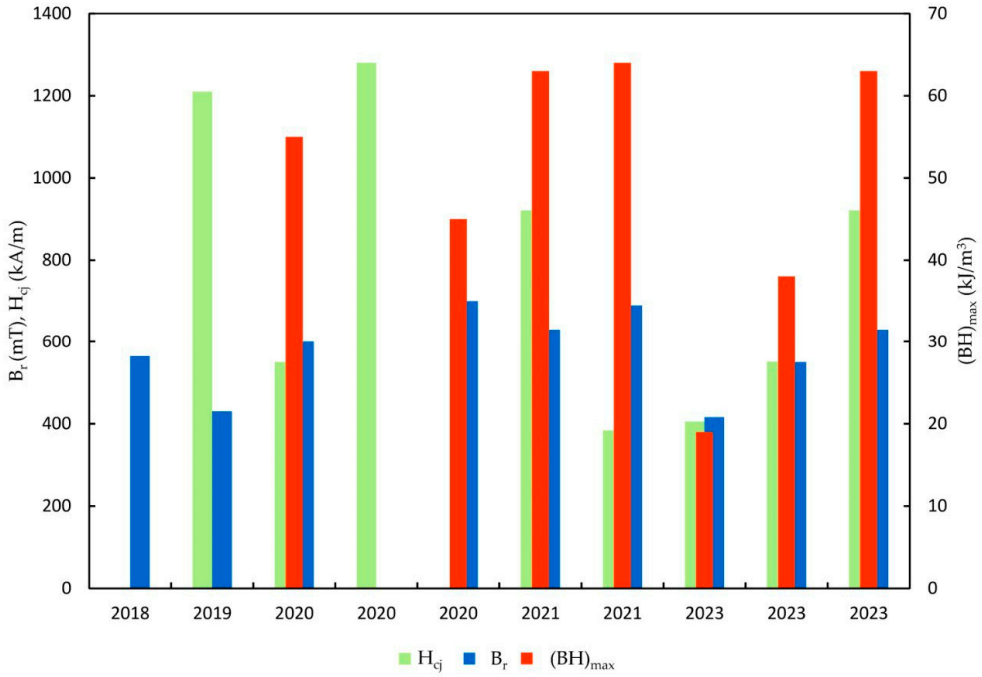


Figure 7. Diagram of magnetic properties of Nd-Fe-B materials synthesized by LPBF.

6. Conclusions

The three-dimensional printing of Nd-Fe-B-based permanent magnets using the LPBF method is a novel and rapidly developing research topic. A lot of progress has been made in this area since 2017, when the first study of $Nd_2Fe_{14}B$ volumetric LPBF samples appeared. Improving the printing quality and magnetic properties has been achieved by various approaches, such as printing process optimization (including specific scanning strategies), the addition of low-melting phases (grain boundary infiltration), the variation in alloy composition, and heat treatments. The three-dimensional printing of high-density samples with complex shapes has already become reality. Comparing conventional methods, AM could decrease the number of obligatory stages of product production. The latest studies show impressive magnetic properties: more than three times the coercivity, compared with values obtained in the first works on this topic. However, remanence increase is still challenging, since there is no approach to forming strong texture and magnetic anisotropy during or after LPBF yet. Thus, a relatively low energy product of 65 kJ/m^3 has been achieved so far, which is lower than that of magnets obtained via conventional methods. Further development of fully dense 3D-printed permanent magnets based on Nd-Fe-B and improvements in their properties through new approaches to microstructure anisotropy formation are expected, which will allow aligned grains to be obtained in the printed material, hence bringing remanence closer to saturation magnetization. Potentially, this could be realized by printing in a high magnetic field, by aligning the particles before laser scanning, or in some other way. Additionally, various combinations of the overlooked approaches to magnetic property improvement could also be implemented to approach the level of conventionally obtained magnets, and excellent performance of additively manufactured hard magnets could be achieved through the precise control of the intergrain exchange interaction among the grains of the $Nd_2Fe_{14}B$ phase.

Author Contributions: Conceptualization, I.P. and M.L.; investigation, L.F.; data curation, S.C.; writing—original draft preparation, M.L. and I.P.; writing—review and editing, I.T.; visualization, I.P.; supervision, I.T. All authors have read and agreed to the published version of the manuscript.

Funding: This study was supported by the Russian Science Foundation, project No. 19-79-30025, https://rscf.ru/en/project/19-79-30025/ URL (accessed on 30 January 2025).

Data Availability Statement: The data presented in this study are available upon request from the corresponding author. The data are not publicly available due to privacy.

Conflicts of Interest: The authors declare no conflicts of interest.

References

1. El-Refaie, A.; Osama, M. High Specific Power Electrical Machines: A System Perspective. *CES Trans. Electr. Mach. Syst.* **2019**, *3*, 88–93. [CrossRef]
2. Ghassemi, M. High Power Density Technologies for Large Generators and Motors for Marine Applications with Focus on Electrical Insulation Challenges. *High Volt.* **2020**, *5*, 7–14. [CrossRef]
3. Matsuura, Y. Demagnetization Process of Nd-Fe-B Sintered and Ferrite Magnets. *IEEJ Trans. Electr. Electron. Eng.* **2025**, *579*, 170854. [CrossRef]
4. Poenaru, I.; Lixandru, A.; Güth, K.; Malfliet, A.; Yoon, S.; Škulj, I.; Gutfleisch, O. HDDR Treatment of Ce-Substituted $Nd_2Fe_{14}B$-Based Permanent Magnet Alloys—Phase Structure Evolution, Intergranular Processes and Magnetic Property Development. *J. Alloys Compd.* **2020**, *814*, 152215. [CrossRef]
5. Gao, Y.; Bai, Y.; Zhu, H.; Liang, W.; Liu, Q.; Dong, H.; Jia, R.; Ma, W. Corrosion Resistance, Mechanical and Magnetic Properties of Cold-Sprayed Al Coating on Sintered NdFeB Magnet. *J. Therm. Spray Technol.* **2021**, *30*, 2117–2127. [CrossRef]
6. Li, Z.; Kedous-Lebouc, A.; Dubus, J.-M.; Garbuio, L.; Personnaz, S. Direct Reuse Strategies of Rare Earth Permanent Magnets for PM Electrical Machines—An Overview Study. *Eur. Phys. J. Appl. Phys.* **2019**, *86*, 20901. [CrossRef]
7. Önal, M.A.R.; Dewilde, S.; Degri, M.; Pickering, L.; Saje, B.; Riaño, S.; Walton, A.; Binnemans, K. Recycling of Bonded NdFeB Permanent Magnets Using Ionic Liquids. *Green Chem.* **2020**, *22*, 2821–2830. [CrossRef]
8. Qiao, Z.; Dong, S.; Li, Q.; Lu, X.; Chen, R.; Guo, S.; Yan, A.; Li, W. Performance Prediction Models for Sintered NdFeB Using Machine Learning Methods and Interpretable Studies. *J. Alloys Compd.* **2023**, *963*, 171250. [CrossRef]
9. Schliesch, T. Injection Molded Permanent Magnets. In *Modern Permanent Magnets*; Elsevier: Amsterdam, The Netherlands, 2022; pp. 209–250.
10. Croat, J.J. Compression Bonded NdFeB Permanent Magnets. In *Modern Permanent Magnets*; Elsevier: Amsterdam, The Netherlands, 2022; pp. 169–208.
11. Ma, B.M.; Herchenroeder, J.W.; Smith, B.; Suda, M.; Brown, D.N.; Chen, Z. Recent Development in Bonded NdFeB Magnets. *J. Magn. Magn. Mater.* **2002**, *239*, 418–423. [CrossRef]
12. Gandha, K.; Ouyang, G.; Gupta, S.; Kunc, V.; Parans Paranthaman, M.; Nlebedim, I.C. Recycling of Additively Printed Rare-Earth Bonded Magnets. *Waste Manag.* **2019**, *90*, 94–99. [CrossRef]
13. Itoh, M.; Masuda, M.; Suzuki, S.; Machida, K. Recycling of Rare Earth Sintered Magnets as Isotropic Bonded Magnets by Melt-Spinning. *J. Alloys Compd.* **2004**, *374*, 393–396. [CrossRef]
14. Zakotnik, M.; Harris, I.R.; Williams, A.J. Possible Methods of Recycling NdFeB-Type Sintered Magnets Using the HD/Degassing Process. *J. Alloys Compd.* **2008**, *450*, 525–531. [CrossRef]
15. Aboulkhair, N.T.; Simonelli, M.; Parry, L.; Ashcroft, I.; Tuck, C.; Hague, R. 3D Printing of Aluminium Alloys: Additive Manufacturing of Aluminium Alloys Using Selective Laser Melting. *Prog. Mater. Sci.* **2019**, *106*, 100578. [CrossRef]
16. Mehrpouya, M.; Tuma, D.; Vaneker, T.; Afrasiabi, M.; Bambach, M.; Gibson, I. Multimaterial Powder Bed Fusion Techniques. *Rapid Prototyp. J.* **2022**, *28*, 1–19. [CrossRef]
17. Ahmadi, M.; Tabary, S.A.A.B.; Rahmatabadi, D.; Ebrahimi, M.S.; Abrinia, K.; Hashemi, R. Review of Selective Laser Melting of Magnesium Alloys: Advantages, Microstructure and Mechanical Characterizations, Defects, Challenges, and Applications. *J. Mater. Res. Technol.* **2022**, *19*, 1537–1562. [CrossRef]
18. Nzengue, A.G.B.; Mpofu, K.; Mathe, N.; Daniyan, I.; Muvunzi, R. An Experimental Investigation of Selective Laser Process Parameters on Aluminium Alloy (AlSi12). *Procedia CIRP* **2023**, *118*, 638–642. [CrossRef]
19. Gullane, A.; Murray, J.W.; Hyde, C.J.; Sankare, S.; Evirgen, A.; Clare, A.T. On the Use of Multiple Layer Thicknesses within Laser Powder Bed Fusion and the Effect on Mechanical Properties. *Mater. Des.* **2021**, *212*, 110256. [CrossRef]
20. Ming, X.; Song, D.; Yu, A.; Tan, H.; Zhang, Q.; Zhang, Z.; Chen, J.; Lin, X. Effect of Heat Treatment on Microstructure, Mechanical and Thermal Properties of Selective Laser Melted AlSi7Mg Alloy. *J. Alloys Compd.* **2023**, *945*, 169278. [CrossRef]

21. Yang, E.; Leary, M.; Lozanovski, B.; Downing, D.; Mazur, M.; Sarker, A.; Khorasani, A.; Jones, A.; Maconachie, T.; Bateman, S.; et al. Effect of Geometry on the Mechanical Properties of Ti-6Al-4V Gyroid Structures Fabricated via SLM: A Numerical Study. *Mater. Des.* **2019**, *184*, 108165. [CrossRef]
22. Rahulan, N.; Sharma, S.S.; Rakesh, N.; Sambhu, R. A Short Review on Mechanical Properties of SLM Titanium Alloys Based on Recent Research Works. *Mater. Today Proc.* **2022**, *56*, A7–A12. [CrossRef]
23. Yin, H.; Li, P. Micropore-Propagation-Based Model of Fatigue Life Analysis of SLM Manufactured Ti-6Al-4V. *Int. J. Fatigue* **2023**, *167*, 107352. [CrossRef]
24. Mubarok, S.; Puspitasari, P.; Andoko, A.; Lubis, A.M.H.S.; Permanasari, A.A.; Abdullah, M.I.H.C. Failure Mechanism on Ti-6Al-4V Material Processed Using Selective Laser Melting (SLM). In Proceedings of the 5th International Conference on Advances in Manufacturing and Materials Engineering: ICAMME, Kuala Lumpur, Malaysia, 9–10 August 2022; Springer: Singapore, 2023; pp. 321–326.
25. Metalnikov, P.; Ben-Hamu, G.; Eliezer, D. Corrosion Behavior of AM-Ti-6Al-4V: A Comparison between EBM and SLM. *Prog. Addit. Manuf.* **2022**, *7*, 509–520. [CrossRef]
26. Lv, Z.; Li, H.; Che, L.; Chen, S.; Zhang, P.; He, J.; Wu, Z.; Niu, S.; Li, X. Effects of HIP Process Parameters on Microstructure and Mechanical Properties of Ti-6Al-4V Fabricated by SLM. *Metals* **2023**, *13*, 991. [CrossRef]
27. Deng, J.; Chen, C.; Liu, X.; Li, Y.; Zhou, K.; Guo, S. A High-Strength Heat-Resistant Al−5.7Ni Eutectic Alloy with Spherical Al3Ni Nano-Particles by Selective Laser Melting. *Scr. Mater.* **2021**, *203*, 114034. [CrossRef]
28. Nagahari, T.; Nagoya, T.; Kakehi, K.; Sato, N.; Nakano, S. Microstructure and Creep Properties of Ni-Base Superalloy IN718 Built up by Selective Laser Melting in a Vacuum Environment. *Metals* **2020**, *10*, 362. [CrossRef]
29. Kaplanskii, Y.Y.; Sentyurina, Z.A.; Loginov, P.A.; Levashov, E.A.; Korotitskiy, A.V.; Travyanov, A.Y.; Petrovskii, P.V. Microstructure and Mechanical Properties of the (Fe,Ni)Al-Based Alloy Produced by SLM and HIP of Spherical Composite Powder. *Mater. Sci. Eng. A* **2019**, *743*, 567–580. [CrossRef]
30. Mazeeva, A.K.; Staritsyn, M.V.; Bobyr, V.V.; Manninen, S.A.; Kuznetsov, P.A.; Klimov, V.N. Magnetic Properties of Fe–Ni Permalloy Produced by Selective Laser Melting. *J. Alloys Compd.* **2020**, *814*, 152315. [CrossRef]
31. Lesyk, D.; Martinez, S.; Pedash, O.; Dzhemelinskyi, V.; Mordyuk, B. Combined Thermo-Mechanical Techniques for Post-Processing of the SLM-Printed Ni-Cr-Fe Alloy Parts. In *Design, Simulation, Manufacturing: The Innovation Exchange*; Springer International Publishing: Cham, Switzerland, 2020; pp. 295–304.
32. Mohamed, A.; Takaichi, A.; Kajima, Y.; Hanawa, T.; Wakabayashi, N. Reusing the Co–Cr–Mo Support Structures of Selective Laser Melted Parts: Evaluation of Mechanical Properties and Microstructures. *Sustain. Mater. Technol.* **2023**, *36*, e00608. [CrossRef]
33. Huang, Z.; Wang, B.; Liu, F.; Song, M.; Ni, S.; Liu, S. Microstructure Evolution, Martensite Transformation and Mechanical Properties of Heat Treated Co-Cr-Mo-W Alloys by Selective Laser Melting. *Int. J. Refract. Met. Hard Mater.* **2023**, *113*, 106170. [CrossRef]
34. Wenbin, L.; Junhao, D.; Xiao, C.; You, W.; Xu, S.; Sai, Z. A 3D-Printed CuNi Alloy Catalyst with a Triply Periodic Minimal Surface for the Reverse Water-Gas Shift Reaction. *J. Mater. Chem. A* **2023**, *12*, 314–320.
35. Sankar, B.; Vinay, C.; Vishnu, J.; Shankar, K.V.; Gokul Krishna, G.P.; Govind, V.; Jayakrishna, A.J. Focused Review on Cu–Ni–Sn Spinodal Alloys: From Casting to Additive Manufacturing. *Met. Mater. Int.* **2023**, *29*, 1203–1228. [CrossRef]
36. Andreiev, A.; Hoyer, K.-P.; Hengsbach, F.; Haase, M.; Tasche, L.; Duschik, K.; Schaper, M. Powder Bed Fusion of Soft-Magnetic Iron-Based Alloys with High Silicon Content. *J. Mater. Process. Technol.* **2023**, *317*, 117991. [CrossRef]
37. Garibaldi, M.; Ashcroft, I.; Lemke, J.N.; Simonelli, M.; Hague, R. Effect of Annealing on the Microstructure and Magnetic Properties of Soft Magnetic Fe-Si Produced via Laser Additive Manufacturing. *Scr. Mater.* **2018**, *142*, 121–125. [CrossRef]
38. Gu, D.; Hagedorn, Y.-C.; Meiners, W.; Meng, G.; Batista, R.J.S.; Wissenbach, K.; Poprawe, R. Densification Behavior, Microstructure Evolution, and Wear Performance of Selective Laser Melting Processed Commercially Pure Titanium. *Acta Mater.* **2012**, *60*, 3849–3860. [CrossRef]
39. Ng, C.C.; Savalani, M.M.; Lau, M.L.; Man, H.C. Microstructure and Mechanical Properties of Selective Laser Melted Magnesium. *Appl. Surf. Sci.* **2011**, *257*, 7447–7454. [CrossRef]
40. Wang, D.; Yu, C.; Ma, J.; Liu, W.; Shen, Z. Densification and Crack Suppression in Selective Laser Melting of Pure Molybdenum. *Mater. Des.* **2017**, *129*, 44–52. [CrossRef]
41. Zhou, L.; Yuan, T.; Li, R.; Tang, J.; Wang, G.; Guo, K. Selective Laser Melting of Pure Tantalum: Densification, Microstructure and Mechanical Behaviors. *Mater. Sci. Eng. A* **2017**, *707*, 443–451. [CrossRef]
42. Ikeshoji, T.-T.; Nakamura, K.; Yonehara, M.; Imai, K.; Kyogoku, H. Selective Laser Melting of Pure Copper. *JOM* **2018**, *70*, 396–400. [CrossRef]
43. Demir, A.G.; Monguzzi, L.; Previtali, B. Selective Laser Melting of Pure Zn with High Density for Biodegradable Implant Manufacturing. *Addit. Manuf.* **2017**, *15*, 20–28. [CrossRef]
44. Song, B.; Dong, S.; Deng, S.; Liao, H.; Coddet, C. Microstructure and Tensile Properties of Iron Parts Fabricated by Selective Laser Melting. *Opt. Laser Technol.* **2014**, *56*, 451–460. [CrossRef]

45. Chowdhury, S.; Yadaiah, N.; Prakash, C.; Ramakrishna, S.; Dixit, S.; Gupta, L.R.; Buddhi, D. Laser Powder Bed Fusion: A State-of-the-Art Review of the Technology, Materials, Properties & Defects, and Numerical Modelling. *J. Mater. Res. Technol.* **2022**, *20*, 2109–2172. [CrossRef]
46. Jaćimović, J.; Binda, F.; Herrmann, L.G.; Greuter, F.; Genta, J.; Calvo, M.; Tomše, T.; Simon, R.A. Net Shape 3D Printed NdFeB Permanent Magnet. *Adv. Eng. Mater.* **2017**, *19*, 50–51. [CrossRef]
47. Gibson, I.; Rosen, D.; Stucker, B.; Khorasani, M. *Additive Manufacturing Technologies*; Springer International Publishing: Cham, Switzerland, 2021; ISBN 978-3-030-56126-0.
48. Müller, K.-H.; Sawatzki, S.; Gauß, R.; Gutfleisch, O. Permanent Magnet Materials and Applications. In *Handbook of Magnetism and Magnetic Materials*; Springer International Publishing: Cham, Switzerland, 2021; pp. 1369–1433.
49. Pelevin, I.A.; Terekhin, E.A.; Ozherelkov, D.Y.; Tereshina, I.S.; Karpenkov, D.Y.; Bochkanov, F.Y.; Chernyshikhin, S.V.; Nalivaiko, A.Y.; Gromov, A.A. New Scanning Strategy Approach for Laser Powder Bed Fusion of Nd-Fe-B Hard Magnetic Material. *Metals* **2023**, *13*, 1084. [CrossRef]
50. Huber, C.; Sepehri-Amin, H.; Goertler, M.; Groenefeld, M.; Teliban, I.; Hono, K.; Suess, D. Coercivity Enhancement of Selective Laser Sintered NdFeB Magnets by Grain Boundary Infiltration. *Acta Mater.* **2019**, *172*, 66–71. [CrossRef]
51. Volegov, A.S.; Andreev, S.V.; Selezneva, N.V.; Ryzhikhin, I.A.; Kudrevatykh, N.V.; Mädler, L.; Okulov, I.V. Additive Manufacturing of Heavy Rare Earth Free High-Coercivity Permanent Magnets. *Acta Mater.* **2020**, *188*, 733–739. [CrossRef]
52. Tosoni, O.; Borges Mendonça, E.; Reijonen, J.; Antikainen, A.; Schäfer, L.; Riegg, S.; Gutfleisch, O. High-Coercivity Copper-Rich Nd-Fe-B Magnets by Powder Bed Fusion Using Laser Beam Method. *Addit. Manuf.* **2023**, *64*, 103426. [CrossRef]
53. Yadroitsev, I.; Bertrand, P.; Smurov, I. Parametric Analysis of the Selective Laser Melting Process. *Appl. Surf. Sci.* **2007**, *253*, 8064–8069. [CrossRef]
54. Périgo, E.A.; Jacimovic, J.; García Ferré, F.; Scherf, L.M. Additive Manufacturing of Magnetic Materials. *Addit. Manuf.* **2019**, *30*, 100870. [CrossRef]
55. MQP-S-11-9-20001. Available online: https://mqitechnology.com/product/mqp-s-11-9-20001/ (accessed on 30 January 2025).
56. Pelevin, I.A.; Ozherelkov, D.Y.; Chernyshikhin, S.V.; Nalivaiko, A.Y.; Gromov, A.A.; Chzhan, V.B.; Terekhin, E.A.; Tereshina, I.S. Selective Laser Melting of Nd-Fe-B: Single Track Study. *Mater. Lett.* **2022**, *315*, 131947. [CrossRef]
57. Mapley, M.; Gregory, S.D.; Pauls, J.P.; Tansley, G.; Busch, A. Influence of Powder Loading Fraction on Properties of Bonded Permanent Magnets Prepared By Selective Laser Sintering. *3D Print. Addit. Manuf.* **2021**, *8*, 168–175. [CrossRef]
58. Lu, Q.; Shao, Y.; Yin, Y.; Chen, H.; Xu, H.; Liu, W.; Liu, M.; Zhong, C.; Yu, X.; Chen, J.; et al. Mass Production of Regenerated Sintered NdFeB Magnets with Improved Magnetic Properties Compared to Original Magnets. *Sustain. Mater. Technol.* **2023**, *36*, e00615. [CrossRef]
59. Bittner, F.; Thielsch, J.; Drossel, W.-G. Microstructure and Magnetic Properties of Nd-Fe-B Permanent Magnets Produced by Laser Powder Bed Fusion. *Scr. Mater.* **2021**, *201*, 113921. [CrossRef]
60. Urban, N.; Huber, F.; Franke, J. Influences of Process Parameters on Rare Earth Magnets Produced by Laser Beam Melting. In Proceedings of the 2017 7th International Electric Drives Production Conference (EDPC), Wuerzburg, Germany, 5–6 December 2017; IEEE: Piscataway, NJ, USA, 2017; pp. 1–5.
61. Goll, D.; Trauter, F.; Loeffler, R.; Gross, T.; Schneider, G. Additive Manufacturing of Textured FePrCuB Permanent Magnets. *Micromachines* **2021**, *12*, 1056. [CrossRef]
62. Akiya, T.; Liu, J.; Sepehri-Amin, H.; Ohkubo, T.; Hioki, K.; Hattori, A.; Hono, K. High-Coercivity Hot-Deformed Nd–Fe–B Permanent Magnets Processed by Nd–Cu Eutectic Diffusion under Expansion Constraint. *Scr. Mater.* **2014**, *81*, 48–51. [CrossRef]
63. Sawatzki, S.; Dirks, A.; Francu, B.; Löwe, K.; Gutfleisch, O. Coercivity Enhancement in Hot-Pressed Nd-Fe-B Permanent Magnets with Low Melting Eutectics. *J. Appl. Phys.* **2014**, *115*, 17A705. [CrossRef]
64. Tang, X.; Chen, R.; Yin, W.; Wang, J.; Tang, X.; Lee, D.; Yan, A. Enhanced Texture in Die-Upset Nanocomposite Magnets by Nd-Cu Grain Boundary Diffusion. *Appl. Phys. Lett.* **2013**, *102*, 072409. [CrossRef]
65. Cui, B.Z.; Zheng, L.Y.; Marinescu, M.; Liu, J.F.; Hadjipanayis, G.C. Textured $Nd_2Fe_{14}B$ Flakes with Enhanced Coercivity. *J. Appl. Phys.* **2012**, *111*, 07A735. [CrossRef]
66. Mishima, C.; Hamada, N.; Mitarai, H.; Honkura, Y. Development of a Co-Free NdFeB Anisotropic Bonded Magnet Produced from the d-HDDR Processed Powder. *IEEE Trans. Magn.* **2001**, *37*, 2467–2470. [CrossRef]
67. Sepehri-Amin, H.; Ohkubo, T.; Nishiuchi, T.; Hirosawa, S.; Hono, K. Coercivity Enhancement of Hydrogenation–Disproportionation–Desorption–Recombination Processed Nd–Fe–B Powders by the Diffusion of Nd–Cu Eutectic Alloys. *Scr. Mater.* **2010**, *63*, 1124–1127. [CrossRef]
68. Chen, F. Recent Progress of Grain Boundary Diffusion Process of Nd-Fe-B Magnets. *J. Magn. Magn. Mater.* **2020**, *514*, 167227. [CrossRef]
69. Toujun, Z.; Bao, W.; Xu, Z.; Zhao, M.; Huang, X.; Wei, W.; Liu, R.; Xie, G. Optimizing Microstructure, Magnetic Properties and Mechanical Properties of Sintered NdFeB Magnet by Double Alloy Method and Grain Boundary Diffusion. *Intermetallics* **2023**, *162*, 108027. [CrossRef]

70. Zhang, B.; Li, Y.; Bai, Q. Defect Formation Mechanisms in Selective Laser Melting. A Review. *Chin. J. Mech. Eng.* **2017**, *30*, 515–527. [CrossRef]
71. Murugan, P.D.; Vijayananth, S.; Natarajan, M.P.; Jayabalakrishnan, D.; Arul, K.; Jayaseelan, V.; Elanchezhian, J. A Current State of Metal Additive Manufacturing Methods: A Review. *Mater. Today Proc.* **2022**, *59*, 1277–1283. [CrossRef]
72. Javidrad, H.R.; Salemi, S. Effect of the Volume Energy Density and Heat Treatment on the Defect, Microstructure, and Hardness of L-PBF Inconel 625. *Metall. Mater. Trans. A* **2020**, *51*, 5880–5891. [CrossRef]
73. Chaudhary, V.; Mantri, S.A.; Ramanujan, R.V.; Banerjee, R. Additive Manufacturing of Magnetic Materials. *Prog. Mater. Sci.* **2020**, *114*, 100688. [CrossRef]
74. Bittner, F.; Thielsch, J.; Drossel, W.-G. Laser Powder Bed Fusion of Nd–Fe–B Permanent Magnets. *Prog. Addit. Manuf.* **2020**, *5*, 3–9. [CrossRef]
75. Skalon, M.; Görtler, M.; Meier, B.; Arneitz, S.; Urban, N.; Mitsche, S.; Huber, C.; Franke, J.; Sommitsch, C. Influence of Melt-Pool Stability in 3D Printing of NdFeB Magnets on Density and Magnetic Properties. *Materials* **2019**, *13*, 139. [CrossRef]
76. Kim, H.-J.; Jang, Y.R.; Lee, H.-S.; Cho, J.-W.; Jang, T.; Eo, D.-R.; Lee, W. Microstructural Investigation of Nanocrystalline Nd-Fe-B Magnets Fabricated by Laser Powder Bed Fusion. *Mater. Charact.* **2024**, *216*, 114228. [CrossRef]
77. Pant, P.; Salvemini, F.; Proper, S.; Luzin, V.; Simonsson, K.; Sjöström, S.; Hosseini, S.; Peng, R.L.; Moverare, J. A Study of the Influence of Novel Scan Strategies on Residual Stress and Microstructure of L-Shaped LPBF IN718 Samples. *Mater. Des.* **2022**, *214*, 110386. [CrossRef]
78. Im, T.; Kim, J.-Y.; Gurung, K.; Meyers, S.; Van Hooreweder, B.; Lee, J.-S.; Kim, J.-K.; Lee, C.S. Impact of Laser Scanning Strategies on Microstructure in Laser Powder Bed Fusion (LPBF) of Nanoparticle-Infused Pre-Alloyed Water-Atomized Iron Powder. *Mater. Sci. Eng. A* **2024**, *891*, 145989. [CrossRef]
79. Dong, H.; He, K.; Meng, X.; Xu, H.; Ming, G.; Du, Y.; Dai, K.; Dong, C. Influence of Laser Powder Bed Fusion Scanning Strategies on the Magnetic and Mechanical Properties of NdFeB. *J. Alloys Compd.* **2025**, *1020*, 179384. [CrossRef]
80. Genç, K.; Toyting, S.; Galindo-Nava, E.; Todd, I.; Mumtaz, K. Laser Powder Bed Fusion of NdFeB and Influence of Powder Bed Heating on Density and Magnetic Properties. *Int. J. Adv. Manuf. Technol.* **2024**, *132*, 5017–5038. [CrossRef]
81. Caniou, R.; Rado, C.; Gaillard, G.-C.; Tosoni, O.; Flament, C.; Garandet, J.-P. Influence of Process Parameters on the Microstructure of Laser Printed NdFeB Alloys. *J. Magn. Magn. Mater.* **2023**, *570*, 170503. [CrossRef]
82. Goll, D.; Trauter, F.; Bernthaler, T.; Schanz, J.; Riegel, H.; Schneider, G. Additive Manufacturing of Bulk Nanocrystalline FeNdB Based Permanent Magnets. *Micromachines* **2021**, *12*, 538. [CrossRef]
83. Du, C.; Zhao, Y.; Jiang, J.; Wang, Q.; Wang, H.; Li, N.; Sun, J. Pore Defects in Laser Powder Bed Fusion: Formation Mechanism, Control Method, and Perspectives. *J. Alloys Compd.* **2023**, *944*, 169215. [CrossRef]
84. du Plessis, A.; Yadroitsava, I.; Yadroitsev, I. Effects of Defects on Mechanical Properties in Metal Additive Manufacturing: A Review Focusing on X-Ray Tomography Insights. *Mater. Des.* **2020**, *187*, 108385. [CrossRef]
85. Jacimovic, J.; Christen, T.; Dénervaud, E. Self-Organized Giant Magnetic Structures via Additive Manufacturing in NdFeB Permanent Magnets. *Addit. Manuf.* **2020**, *34*, 101288. [CrossRef]
86. Wu, J.; Aboulkhair, N.T.; Robertson, S.; Zhou, Z.; Bagot, P.A.J.; Moody, M.P.; Degano, M.; Ashcroft, I.; Hague, R.J.M. Amorphous-Crystalline Nanostructured Nd-Fe-B Permanent Magnets Using Laser Powder Bed Fusion: Metallurgy and Magnetic Properties. *Acta Mater.* **2023**, *259*, 119239. [CrossRef]
87. Yao, B.; Kang, N.; Li, X.; Li, D.; Mansori, M.E.; Chen, J.; Yang, H.; Tan, H.; Lin, X. Toward Understanding the Microstructure Characteristics, Phase Selection and Magnetic Properties of Laser Additive Manufactured Nd-Fe-B Permanent Magnets. *Int. J. Extrem. Manuf.* **2024**, *6*, 015002. [CrossRef]
88. The Vocabulary of Magnetism. Available online: https://www.arnoldmagnetics.com/wp-content/uploads/2017/10/Vocabulary-of-Magnetism.pdf (accessed on 30 January 2025).
89. Gutfleisch, O. Controlling the Properties of High Energy Density Permanent Magnetic Materials by Different Processing Routes. *J. Phys. D Appl. Phys.* **2000**, *33*, R157–R172. [CrossRef]
90. Sugimoto, S. Current Status and Recent Topics of Rare-Earth Permanent Magnets. *J. Phys. D Appl. Phys.* **2011**, *44*, 064001. [CrossRef]
91. Nakamura, H.; Hirota, K.; Shimao, M.; Minowa, T.; Honshima, M. Magnetic Properties of Extremely Small Nd-Fe-B Sintered Magnets. *IEEE Trans. Magn.* **2005**, *41*, 3844–3846. [CrossRef]
92. He, J.; Cao, J.; Yu, Z.; Song, W.; Yu, H.; Hussain, M.; Liu, Z. Grain Boundary Diffusion Sources and Their Coating Methods for Nd-Fe-B Permanent Magnets. *Metals* **2021**, *11*, 1434. [CrossRef]
93. Rong, C.; Shen, B. Nanocrystalline and Nanocomposite Permanent Magnets by Melt Spinning Technique. *Chin. Phys. B* **2018**, *27*, 117502. [CrossRef]
94. Cannesan, N.; Harris, I.R. Aspects of NdFeB HDDR Powders: Fundamentals and Processing. In *Bonded Magnets*; Springer: Dordrecht, The Netherlands, 2003; pp. 13–36.

95. Takeshita, T. Magnetic Properties and Microstructures of the NdFeB Magnet Powder Produced by the HDDR Process(IV). In *Proceedings of the 11th International Workshop on Rare-Earth Magnets and Their Applications*; Carnegie Mellon University: Pittsburgh, PA, USA, 1990; p. 49.
96. Sato, T.; Oka, N.; Ohsuna, T.; Kaneko, Y.; Suzuki, S.; Shima, T. Enhancement of Coercivity for Nd-Fe-B Thin Films by the Infiltration of Nd-Cu Alloy Cap Layer. *J. Appl. Phys.* **2011**, *110*, 023903. [CrossRef]
97. Chang, B.; Du, D.; Yi, C.; Xing, B.; Li, Y. Influences of Laser Spot Welding on Magnetic Property of a Sintered NdFeB Magnet. *Metals* **2016**, *6*, 202. [CrossRef]
98. Schäfer, L.; Skokov, K.; Liu, J.; Maccari, F.; Braun, T.; Riegg, S.; Radulov, I.; Gassmann, J.; Merschroth, H.; Harbig, J.; et al. Design and Qualification of Pr–Fe–Cu–B Alloys for the Additive Manufacturing of Permanent Magnets. *Adv. Funct. Mater.* **2021**, *31*, 2102148. [CrossRef]

Disclaimer/Publisher's Note: The statements, opinions and data contained in all publications are solely those of the individual author(s) and contributor(s) and not of MDPI and/or the editor(s). MDPI and/or the editor(s) disclaim responsibility for any injury to people or property resulting from any ideas, methods, instructions or products referred to in the content.